INTEGRATING SPECTRAL AND TEXTURE INDICES WITH MACHINE LEARNING FOR RICE LEAF AREA INDEX (LAI) ESTIMATION IN SUPHAN BURI, THAILAND

***Kritchayan INTARAT*[1,2], *Paramaporn NETSAWANG*[3], *Supatthra NARAWATTHANA*[3], *Chayapol PROMAOH*[1], and *Saruda CHUENKAMOL*[1,2]**

DOI: 10.21163/GT_2025.201.15

ABSTRACT

This study presents unmanned aerial vehicle (UAV)-based remote sensing to estimate the leaf area index (LAI) in rice fields, across multiple growth stages, by comparing univariate and multivariate methodologies. Univariate models focus on evaluating the performance of individual vegetation indices (VIs), color indices (CIs), and normalized difference texture indices (NDTIs). In contrast, multivariate approaches employ feature selection via recursive feature elimination (RFE) with ensemble machine learning (ML) models: random forest regressor (RFR), gradient boosting regressor (GBR), and eXtreme gradient boosting regressor (XGBR). Dimensionality reduction techniques such as principal component regression (PCR) and partial least squares regression (PLSR) are also employed. Results demonstrate that when associated with stage-specific complexities, NDTI(REsem, Rcor), using a univariate model (XGBR) achieves the highest R^2 value of 0.91 and records the lowest RMSE at 0.38, in the panicle initiation stage. Across all stages, NDTI(Rmean, Bdis) is seen to deliver a high R^2 value of 0.81 while reaching a higher value of 1.20 RMSE than in the specific stages. When associated with multivariate models, CIs indicate the highest accuracy associated with RFE. In this case, five features, out of ten selected, attained 0.88 R^2 and 0.94 RMSE. These findings highlight the potential of integrating UAV-based multivariate approaches in precision agriculture for improved, stage-specific LAI estimation.

Key-words: *Vegetation indices; Color indices; Texture indices; Leaf Area Index; UAV; Machine learning*

1. INTRODUCTION

In photosynthesis, plant leaves are crucial as they convert light into chemical energy. Plant leaves are often used as a factor in plant physical analysis to examine growth and productivity (Fukuda et al., 2021). In agricultural crop studies, the leaf area of plants is an essential indicator of the dry-weight ratio, making it a fundamental parameter (Hikosaka, 2005). In 1947, Watson developed the leaf area index (LAI), quantifying the total leaf surface area per unit ground area. LAI is a crucial indicator of crop growth, plant health, and biomass estimation, particularly for crops with broad, flat leaves like rice, wheat, and maize (Bréda, 2003; Kappas & Propastin, 2012). Due to its importance, LAI is widely used in agricultural monitoring, forestry assessments, and ecological studies (Yan et al., 2019). However, rice observation is still associated with traditional management and monitoring tools. Conventional methods employed for measuring LAI are known to be time-consuming and require considerable effort. Additionally, the destructive field sampling required by such methods could lead to many discrepancies (Abdullah et al., 2019; Li et al., 2019; Fukuda et al., 2021; Afrasiabian et al., 2022).

In the global rice market, Thailand has established itself as a prominent player consistently ranking among the top three rice-exporting countries (Singkawat and Intarat, 2024). The rice industry has been the focus of various organizations, with much attention given to rice yield prediction and related aspects. As for LAI estimation, recent advancements have shifted towards using non-invasive,

[1]*Research Unit in Geospatial Applications (Capybara Geo Lab), Faculty of Liberal Arts, Thammasat University, Thailand. (KI) intaratt@tu.ac.th, (CP) st124908@ait.asia*

[2]*Dep. of Geography, Fac. of Liberal Arts, Thammasat University, Thailand. (SC) saruda.chu@dome.tu.ac.th*

[3]*Thailand Rice Science Institute (TRSI), Rice Department, Thailand. (PN) paramaporn.n@rice.mail.go.th, (SN) supatthra.n@rice.mail.go.th*

large-scale methods. Remote sensing provides a fast and non-destructive way to estimate LAI over large areas, making it more efficient than traditional field measurement. This monitoring tool provides a straightforward, dependable, real-time, and non-destructive approach for acquiring LAI from rice fields (Yuan et al., 2017; Abdullah et al., 2019). In the context of satellite imagery, optical sensors often face limitations, such as cloud interference and low image resolution, which reduce their effectiveness for monitoring crops. Such images often hinder large-scale studies (Li et al., 2019). Airborne-based unmanned aerial vehicle (UAV) is a promising platform for LAI observation in rice cultivation (Li et al., 2019; Yang et al., 2021). With the advancement of sensor technology, several sensors such as multispectral, hyperspectral, plus light detection and ranging (LiDAR) are now equipped on UAVs (Zhang et al., 2022a). Of late, commercial-grade UAVs have become affordable, making multispectral cameras a standard tool. Apart from rice, this cutting-edge vehicle has been applied to other crops e.g. maize (Liu et al., 2023), sugarcane (Sanches et al., 2018), soybean (Zhang et al., 2022b), wheat (Zhu et al., 2019), and sugar beet (Cao et al., 2020): all have reported success in the improvement of predictive performance.

The utilization of vegetation indices (VIs) and color indices (CIs) has demonstrated their effectiveness in predicting the LAI of rice paddies (Yang et al., 2021; Wang et al., 2019b). Common vegetation indices, such as the normalized difference vegetation index (NDVI) and enhanced vegetation index (EVI), can analyze how plants reflect light to estimate their health and biomass. These indices offer vital insights into plant growth and photosynthetic activity, making them valuable tools for LAI estimation. CIs, derived from the visible spectrum, are seen to harness variations in green, red, and blue bands to quantify leaf area and chlorophyll content. This strategy is particularly useful in detecting subtle changes in leaf pigmentation indicative of plant health and stress levels (Li et al., 2019). Across different growth stages, combining both VIs and CIs can improve the accuracy of LAI prediction. Studies have demonstrated that integrating these indices with machine learning (ML) algorithms greatly enhance prediction accuracy by considering the complex interactions between spectral data and plant physiology (Wang et al., 2011; Yuan et al., 2017). By utilizing these indices, precise monitoring and management of rice crops can be achieved, ensuring optimal growth conditions, thereby amplifying yield predictions. Previous studies have indicated that while spectral data from UAV imagery is most effective, intrinsic spatial details such as texture exhibit significant potential for comprehensive crop observation (Li et al., 2019; Zheng et al., 2019).

The progress in texture analytical techniques has paved the way for more efficient and scalable approaches. One promising method is the utilization of normalized difference texture indices (NDTIs), which employ spatial texture information from remote sensing imagery to predict LAI (Li et al., 2019; Zheng et al., 2019). NDTIs are based on methods of texture analysis that measure spatial differences in image intensity or color. In contrast to standard VIs that mainly use spectral reflectance values, NDTI considers textural patterns, which makes it especially valuable for diverse crop canopies like rice. Li et al. (2019) have integrated texture analysis to construct NDTIs and combined them with CIs obtained from UAV images. When incorporated with an ML algorithm, this combination exhibited robust prediction (Li et al., 2019). Zou et al. (2024) investigated several VIs and performed texture analysis via UAV images to create indices by merging wavelet texture and spectral data. Integrating spectral and textural information can deliver more accurate LAI estimation than using VIs alone. Moreover, analyzing image texture patterns helps detect changes in plant structure and leaf distribution, which are essential for estimating LAI (Yang et al., 2021). However, only a few works demonstrate texture analysis techniques in LAI estimation (Li et al., 2019). Future research is necessary to fully understand the estimation of LAI, using information, spectral and textural, from aerial images taken by commercial-grade UAVs with multispectral sensors.

This work aims to evaluate and compare the efficacy of various spectral indices, namely VIs, CIs, and NDTIs, in predicting LAI. The investigation employs univariate and multivariate regression analyses to assess the enhancement potential of these indices individually and in combination with spectral and textural attributes for the accurate estimation of LAI, across different growth stages of rice based on UAV imagery. Predictive performance is finally quantified by the coefficient of determination (R^2) and the root mean square error (RMSE).

2. STUDY AREA

Recently, an experiment was recently conducted at the Thailand Rice Science Institute (TRSI) in Suphan Buri Province, central Thailand. This region is famous for its traditional rice cultivation and offers four different rice crops (Singkawat and Intarat, 2024). It is located at 14°28’37.8” latitude North and 100°05’18.7” longitude East (**Fig. 1**). Topographical characteristics of the region denote a flat terrain with a slight slope from the western to southeastern region. Altitude ranges from 3 to 10 m above mean sea level. Experimental areas experience a hot, windless, and overcast rainy season. The dry season, in contrast, is characterized by humidity and partly cloudy weather, with high temperatures throughout the year. Temperature varies between 20° to 37°C, rarely falling below 17°C or exceeding 40°C.

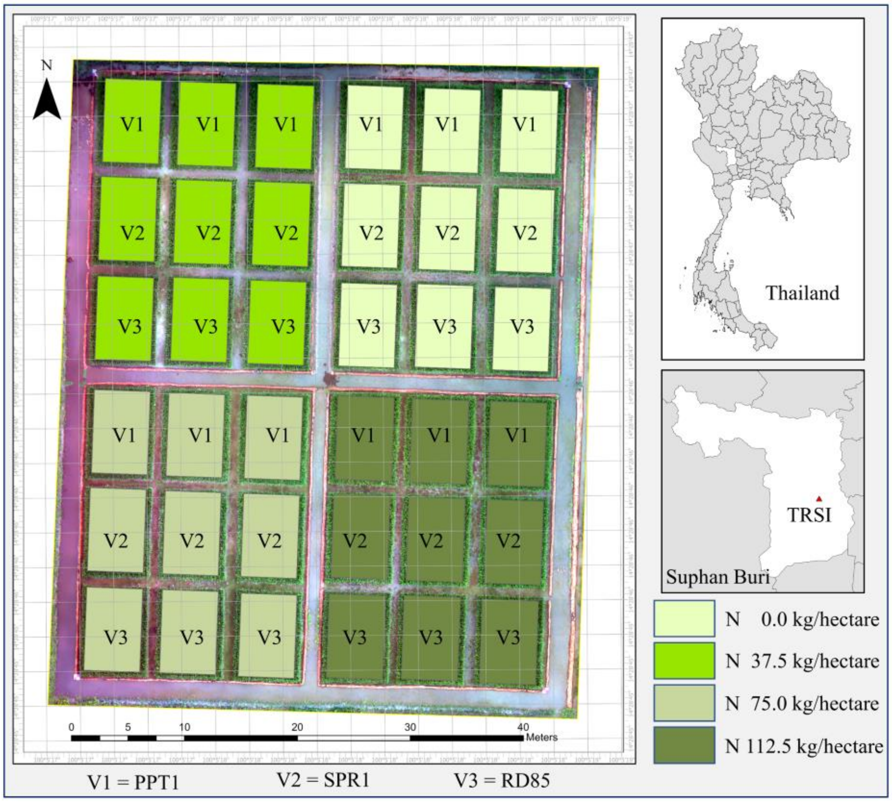

Fig. 1. The study area at the Thailand Rice Science Institute (TRSI), Suphan Buri, Thailand. The experimental plots were manually transplanted, and UAV flights were conducted at specific growth stages, under controlled conditions.

Total annual precipitation, in Suphan Buri, ranges from 900 to 1,200 mm, except in some areas of the western region, where it exceeds 1,200 mm. Rainfall in Suphan Buri originates from the southwest monsoon during the rainy season. The highest precipitation of rainfall is in September, with a record of 190.4 mm per day in 2005. The Tha Chin River, also known as the Suphan Buri River, courses through the eastern side of the province, with dense rice cultivation on both sides of the river. Due to adequate irrigation, rice crops are classified into four categories: single, double, two-and-a-half, and triple (Kamthonkiat et al., 2005). Our field investigation, conducted from August to October 2024, coincided with the single-crop-rice cultivation period.

3. DATA AND METHODS

3.1. Experimental design and field observations

The investigation entailed manual transplanting rice and applying varying nitrogen fertilization rates, rice varieties, and growth stages. Field samples were arranged in a block design with three replicates (36 plots). Each plot revealed 48 m^2 (6 × 8) m^2, containing 1,200 LAI destructive random sampling bundles. In each block, three rice varieties (PPT1, SPR1, and RD85) were cultivated. The experiment involved four nitrogen applications (0.0, 37.5, 75.0, 112.5 kg N $hectare^{-1}$) with the constant rate (37.5 kg $hectare^{-1}$) per application of P and K. LAI was estimated via the leaf areas of all three bundles of rice, using the relationship explained by: $LAI = \frac{LA}{3} \times \rho$, where LA refers to the leaf areas of the three sampling bundles of rice, and ρ represents the density of cultivation, which had 25 bundles m^{-2} in each experimental plot.

Data collection was divided into four stages, based on physical growth characteristics viz. tillering stage (TL), panicle initiation stage (PI), booting stage (BT), and flowering stage (FW), as shown in **Table 1**. In total, the sample size for all stages was 144 samples. At each stage, the rice's leaf area was measured, using LI-3000C portable leaf area meter (LI-COR, Lincoln, NE, United States). Three samples were taken from each plot to calculate the average LAI, at every stage. Finally, the data from all four growth stages were combined for further analysis.

Table 1.

Rice sampling data.

Growth stage (Days After Sowing; DAS)	Transplanting Date	Data collecting Date
Tillering stage: TL (45 DAS)	22 July 2024	16 August 2024
Panicle initiation stage: PI (60 DAS)		27 August 2024
Booting stage: BT (75 DAS)		15 September 2024
Flowering stage: FW (95 DAS)		2 October 2024

3.2. Multispectral image acquisition using UAV

During the experiment, field information for rice over four growth stages used a multi-rotor UAV: namely, the Phantom 4 Multispectral RTK model (DJI-Innovations Inc. based in Shenzhen, China). The UAV was equipped with a sensor offering five spectral bands: blue (B), green (G), red (R), red-edge (RE), and near-infrared (NIR), each with a resolution of 2.08 megapixels, supported by a 3-axis stabilized gimbal. The images captured had a resolution of 1,600 × 1,300 pixels, enabling detailed and precise field observations. The RTK system provided ±0.1 m accuracy for positioning, which can be further enhanced by incorporating ground control points (GCPs). For this experiment, the sensing height was set at 30 m, achieving a ground sampling distance (GSD) of 1.60 cm. The flight plan was designed, using DJI GS Pro, setting the aircraft speed at 1.8 m/s with an 80% overlap for both forward and side coverage, resulting in a shutter interval of 2.3 s. The camera ISO was set to 100, and the fixed exposure was adjusted due to each flight's lighting conditions. Field observations were conducted between 10:00 and 11:30 a.m., under conditions of low wind speed and clear skies. Image preprocessing tasks, such as alignment, georeferencing, dense cloud generation, and ortho-mosaicking were carried out, using Agisoft LLC (ST. Petersburg, Russia) and ENVI/IDL software (Harris Geospatial Solutions, Inc., Broomfield, CO, USA).

3.3. Soil background removal

Several rice stages are seen to have background issues, such as noise that could be contained in the calculation. A discrepancy may occur due to local spectral heterogeneity (Liu et al., 2023). In the precision of crop monitoring, and yield prediction, a preprocessing step is critical (Xue & Su, 2017). Liu et al. (2021) reported that soil and non-soil background removal revealed a relative RMSE of 3.02%. Such a vital step is seen to improve the model's accuracy. In this experiment, red green blue vegetation index (RGBVI) was employed to extract the leaf area of rice from the soil, at each growth stage. In **Table 2**, empirical threshold values, corresponding to the critical rice growth stages, are outlined.

Table 2.

Empirical threshold values of RGBVI.

Growth stage (Days After Sowing; DAS)	The empirical threshold value of RGBVI
Tillering stage: TL (45 DAS)	0.40
Panicle initiation stage: PI (60 DAS)	0.40
Booting stage: BT (75 DAS)	0.35
Flowering stage: FW (95 DAS)	0.30

Table 2 incorporated these empirical threshold values to distinguish between rice's leaves and soil background, constructing the binary mask image (**Fig. 2**) and removing the background pixels from each rice's stage. Pixels that only contain the reflectance of leaves will be used to calculate Vis, CIs, and NDTIs, respectively.

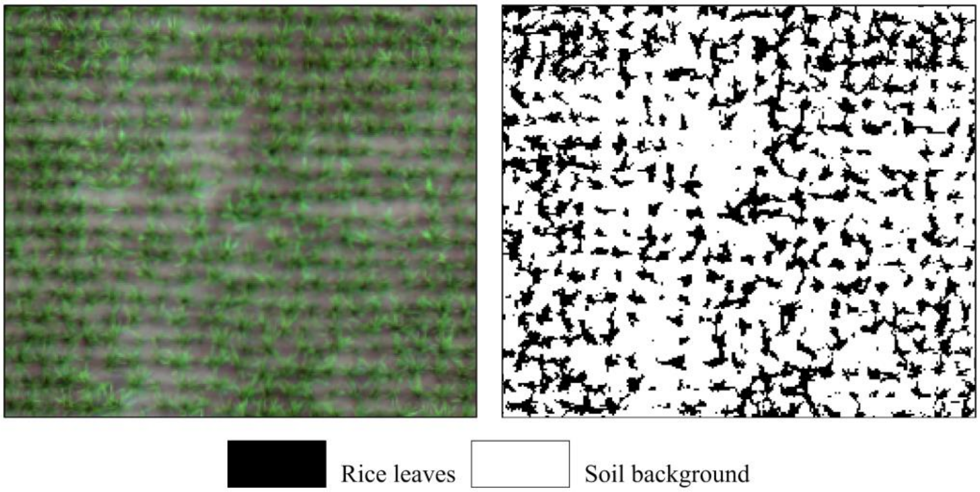

Fig. 2. An example of the RGBVI threshold segmentation applied for soil background removal. The RGBVI threshold values were empirically determined for each growth stage to minimize soil interference.

3.4. Color indices (CIs) and vegetation indices (VIs)

After completing the necessary image preprocessing tasks and extracting the soil background, using ENVI/IDL, UAV images of rice, at different growth stages, were utilized to create Cis and Vis. These processes involved extracting the reflectance values of rice leaves to calculate ratios based on specific equations. To generate CIs, it is essential to calculate the normalized values of r, g, and b bands from the RGB image data first. This normalization can enhance reflectance effectiveness, compared to general RGB images. The bands (r, g, and b) are structured and can be expressed, as follows:

$$r = \frac{R}{R+G+B} \tag{1}$$

$$g = \frac{G}{R+G+B} \tag{2}$$

$$b = \frac{B}{R+G+B} \tag{3}$$

where r, g and b is the pixel value in the R, G, and B bands, respectively.

It is noted that VIs are sophisticated analytical instruments for qualitative and quantitative vegetation assessment that capture multispectral image data. These indices are derived by applying specific mathematical formulas to data obtained from different wavelengths, generating numerical indices (Gong et al., 2021). This method reduces the impact of lighting variability during image capture, thus increasing data accuracy and reliability. Owing to their enhanced reliability and precision, VIs have found widespread application in a myriad of research domains, notably in the quantitative assessment of vegetation cover, the evaluation of plant health, and the measurement of chlorophyll concentrations (Gong et al., 2021; Yang et al., 2021). This study incorporates both CIs and VIs for analysis. In **Table 3,** the specific indices employed are given.

Table 3.

Indices CIs and VIs, as constructed by visible and multi-spectral bands.

Rational variables	Formulas	References
CIs		
Visible Atmospherically Resistant Index (VARI)	$(g-r)/(g+r-b)$	Gitelson et al. (2002)
Excess Green Vegetation Index (ExG)	$2g-r-b$	Woebbecke et al. (1995)
Excess Red Vegetation Index (ExR)	$1.4r-g$	Meyer et al. (2008)
Excess Blue Vegetation Index (ExB)	$1.4b-g$	Mao et al. (2003)
Excess Green – Excess Red Vegetation Index (ExGR)	$E\times G-E\times R$	Neto et al. (2004)
Normalized Green-Red Difference Index (NGRDI)	$(g-r)/(g+r)$	Tucker et al. (1979)
Woebbecke index (WI)	$(g-b)/(r-g)$	Woebbecke et al. (1995)
Kawashima Index (IKAW)	$(r-b)/(r+b)$	Kawashima et al. (1998)
Green Leaf Algorithm (GLA)	$(2g-r-b)/(2g+r+b)$	Louhaichi et al. (2001)
Red Green Blue Vegetation Index (RGBVI)	$(g^2-b*r)/(g^2+b*r)$	Bendig et al. (2015)
Vegetative (VEG)	$g/(r^{0.667}b^{(1-0.667)})$	Hague et al. (2006)
VIs		
Green Chlorophyll index (CIg)	(NIR / G) – 1	Gitelson et al. (2003)
Ratio Vegetation Index (RVI)	NIR / R	Rouse et al. (1974)
Red-edge Chlorophyll index (CIre)	(NIR / R) – 1	Gitelson et al. (2003)
Green Normalized Difference Vegetation Index (GNDVI)	(NIR – G) / (NIR + G)	Gitelson et al. (1996)
Normalized Difference Vegetation Index (NDVI)	(NIR – R) / (NIR + R)	Rouse et al. (1973)
Normalized Difference Red-edge Vegetation Index (NDRE)	(NIR – RE) / (NIR + RE)	Fitzgerald et al. (2010)
MERIS terrestrial Chlorophyll Index (MTCI)	(NIR – RE) / (RE – R)	Dash & Curran (2004)
Optimized Soil-Adjusted Vegetation Index (OSAVI)	1.16(NIR – RE) / (NIR + RE + 0.16)	Rondeaux et al. (1996)
Two-band Enhanced Vegetation Index (EVI2)	2.5(NIR – R) / (1 + NIR + 2.4 × R)	Jiang et al. (2008)

3.5. Analysis of the image's texture

The grey level co-occurrence matrix (GLCM) has emerged as a main efficacious tool in statistical analysis, particularly for texture extraction within the domain of UAV multispectral imagery. This methodology is pivotal in quantifying LAI concerning rice cultivation (Zhang et al., 2021). Embedded within its operational framework, GLCM facilitates the computation of grey-level texture values among pixels confined within a designated window, subsequently enabling the extraction of relevant statistical characteristics.

Utilization of the ENVI/IDL software suite permits the computation of eight fundamental GLCM textures i.e. mean (mea), variance (var), homogeneity (hom), contrast (con), dissimilarity (dis), entropy (ent), second moment (sec), and correlation (cor), all within the confines of a 3x3 pixel matrix (Li et al., 2019). These extracted GLCM metrics serve as fundamental elements in deriving NDTI. This measure substantially augments the efficacy of texture analysis. This step is seen to augment LAI evaluation in rice and prepares data for further analysis (Zheng et al., 2020). The computation of NDTI is concisely outlined, as in Eq. (4), providing a methodological roadmap for subsequent analysis:

$$NDTI\ (T_1, T_2) = \frac{(T_1 - T_2)}{(T_1 + T_2)} \tag{4}$$

where T_1 and T_2 represent a pair of two different grey-level textures.

3.6. Random forest regressor (RFR)

The RFR model represents a significant advancement over the decision tree model. This model employs bootstrap aggregating and random subspace selection to classify or predict independent datasets (Breiman, 2001). Random Forests' versatility in handling classification and regression tasks has been noted, underpinned by the model's approach of integrating multiple decision trees to form a cohesive "forest." Each constituent tree contributes to the classification and grouping of data, with the aggregate outcome determined by identifying the mode of the results across the ensemble of trees, thus enhancing both the accuracy and precision of the model (Zhang et al., 2022a). RFR can be described, as follows:

$$\hat{y}(x) = \frac{1}{T}\sum_{t=1}^{T} h_t(x) \tag{5}$$

where T is the total number of trees, $h_t(x)$ represents the prediction of the t^{th} tree for input x, $\hat{y}(x)$ refers to the final prediction made by random forest.

The RFR model addresses common pitfalls such as overfitting and multicollinearity, promoting a more robust and reliable predictive performance (Li et al., 2019). To boost model performance, it is essential to adjust its hyperparameters based on the dataset. Critical among these hyperparameters are the number of trees within the forest, the depth of each tree, and the minimum number of samples required at each leaf node. These parameters are vital for optimizing the model's performance, as evident in recent empirical studies (Li et al., 2019; Zhang et al., 2022a; Yuan et al., 2023). The precise adjustment of these hyperparameters can significantly enhance the predictive accuracy of the RFR model, making it a powerful tool in data science and machine learning.

3.7. Gradient boosting regressor (GBR)

GBR constitutes a pivotal methodology for addressing classification and regression challenges (Liu et al., 2021b). GBR works by optimizing error functions, thereby building an accurate predictive model. This objective is realized through amalgamating numerous subsidiary prediction models, notably decision trees. Subsequent iterations refine these decision trees by diminishing the discrepancies between predicted outcomes, and actual observations: methodological refinements are substantiated and reiterated. A major advantage of GBR is its ability to model complex relationships between variables. Moreover, its algorithmic design exhibits proficiency in managing voluminous datasets, gracefully accommodating instances of missing data, and upholding resilience in the face of outlier data points (Liu et al., 2021b). The mathematical underpinning of the GBR model is encapsulated in Eq. (6), offering a quantifiable representation of its operational mechanics:

$$f_m(x) = f_{m-1}(x) + \eta\rho_m g_m(x) \tag{6}$$

where $f_m(x)$ is the updated model after m iteration, $f_{m-1}(x)$ is the model from the previous iteration, η is the learning rate that handles the effect of each new tree, ρ_m is the step size determined by minimizing the loss function, and $g_m(x)$ is the new regression tree fitted to the residuals of the previous model.

3.8. eXtreme gradient boosting regressor (XGBR)

Chen and Guestrin (2016) proposed XGBR as a scalable tree-boosting system. In particular, XGBR is seen to enhance the gradient boosting algorithm, using Taylor expansion to obtain the second derivative as an independent variable (Liu et al., 2021a). XGBR effectively reduces the computational complexity of creating segmentation trees, improves operational speed, and increases prediction accuracy (Wang et al., 2022). Due to its proficiency in these areas, XGBR is widely applied in model construction (Zhang et al., 2022a; Chen and Guestrin, 2016). It works by combining multiple "weak" learners to create a "strong" learner through additive learning (Liu et al., 2021a). In Eq. (7), the prediction function is represented. For estimating the fitting effect, the loss function is given, as in Eq. (8):

$$y_{i,p} = \sum_{k=1}^{K} f_k(x_i) \quad (7)$$

where $y_{i,p}$ is the predicted value, $f(x_i)$ is a learner, x_i is the input data, and K is the number of learners.

$$\psi = \sum_{i=1}^{n} l(y_{i,p}, y_i) + \sum_{k=1}^{k} \Omega(f_k) \quad (8)$$

where $l(y_{i,p}, y_i)$ is the function that shows the residual size between the predicted and observed values. $\Omega(f_k)$ is the regularization, which shows the complexity of the model.

3.9. Principal component regressor (PCR) and partial least squares regressor (PLSR)

When dealing with many predictors, multicollinearity can occur in the ordinary least square prediction. To overcome such issues, the principal component regression (PCR) is applied. PCR is a technique that combines principal component analysis (PCA) with linear regression. First, PCA reduces the dimensions of the dataset while retaining as much variance as possible. Subsequently, linear regression employs the chosen principle components as predictors within a regression model. To mitigate the risk of multicollinearity, PCR identifies uncorrelated principal components, preventing complications such as exaggerated standard errors (Li et al., 2019). Consequently, it can alleviate overfitting, particularly in scenarios with several predictors.

Another method for handling high-dimensional data is partial least squares regression (PLSR). Unlike PCR, PLSR simultaneously reduces predictors and performs regression. PLSR first standardizes the data to prevent larger factors from dominating the analysis. Subsequently, it produces additional variables (latent variables or components) that are linear combinations of the original predictors. To clarify the predictors' variance, latent variables are chosen, thus bolstering the covariance with the response variables (Yuan et al., 2023). However, there are some concerns about using those two models. Interpreting PCR results can be a bit challenging because the components are linear combinations of the original variables. It is harder to attribute the effect of individual variables directly. Besides, the PLSR model provides coefficients that relate the original predictors to the response. On the other hand, the interpretation can be complex regarding the combinations of the original predictors in latent variables.

3.10. Univariate and multivariate regressors

CIs, VIs, and NDTIs, at each rice growth stage, were used as input variables for univariate regression models. To construct the NDTIs, eight GLCM textures were analyzed. Then, each pair of NDTIs was examined to determine the relationship between such indices and LAI. The investigation identified the top ten NDTIs with the most substantial relationship regarding the statistical test. As for CIs and Vis, to test the performance of each index for estimating LAI at specific stages and across all growth stages, all indices were incorporated into the ML models: RFR, GBR, and XGBR were employed. Herein, the analysis helped us determine which index most correlated with LAI field observations. The best three results, of each CIs, VIs, and NDTIs, were selected.

Further, multivariate regression models, CIs, VIs, and NDTIs, across the entire growth stages of rice, were used as input variables (Li et al., 2019). The models tested included RFR, GBR, XGBR, PCR, and PLSR. The models were optimized to estimate the most accurate LAI (Liu et al., 2023) by acquiring the best combination of hyperparameters, using Gridsearch in the Scikit-learn Python library (Fabian, 2011). For PCR and PLSR, the number of retained components was determined based on cross-validation, balancing model complexity and predictive accuracy (Zheng et al., 2020). In **Table 4,** hyperparameter details are presented.

Table 4.

Hyperparameters for RFR, GBR, XGBR, PCR and PLSR.

Models	Parameters
RFR	'n_estimators': [500, 800, 1000], 'max_depth': [1, 2, 3, 5], 'min_samples_leaf': [1, 2, 3]
GBR	'n_estimators', 'max_depth', 'min_samples_leaf'
XGBR	'n_estimators', 'max_depth', 'min_child_weight'
PCR	The number of components
PLSR	The number of components

In **Table 4**, the set of hyperparameters, considered in the optimization of the ML multivariate models, are outlined. The multivariate variables were divided into several groups: CIs, VIs, NDTIs, and their combinations, such as CIs + VIs, CIs + NDTIs, VIs + NDTIs, and CIs + VIs + NDTIs, respectively. As previously mentioned, the regression models were applied to assess which combinations of multivariate indices best explain the variation in LAI. In **Fig. 3**, a flowchart of the experiment is depicted.

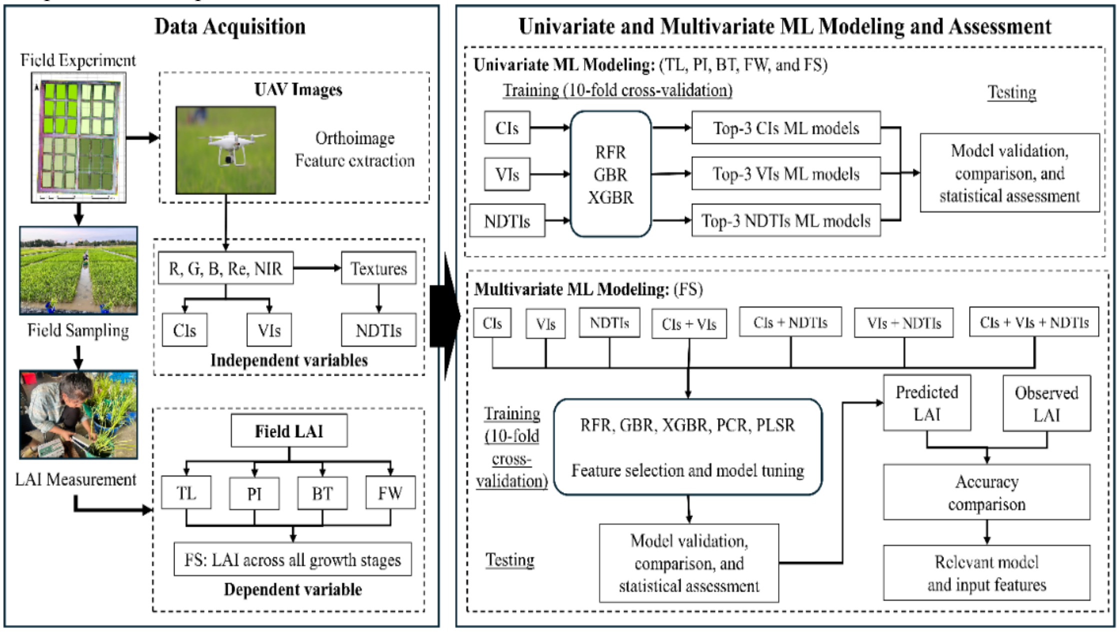

Fig. 3. The methodological framework, including UAV data acquisition, preprocessing (radiometric and geometric corrections), spectral index computation, texture extraction, and machine learning modeling.

According to multivariate model training, feature selection is associated with enhancing the predictive accuracy of these models and reducing the complexity of input features (Zeng et al., 2009; Darst et al., 2018). In this case, the recursive feature elimination (RFE) was applied to ML model training. RFE is an iterative process that utilizes an external estimator to rank features based on their importance (Chan et al., 2022). RFE can remove the least significant features and can re-evaluate the model until the desired number of top-performing features is obtained. Therefore, the model is able to focus on only the most relevant features to improve performance and computational efficiency (Shrestha, 2020). Based on the available UAV equipment and specific requirements, users can select the best and most appropriate approach by providing univariate and multivariate ML models.

3.11. Statistical analysis

To evaluate the predictive performance of each model, the input data comprising CIs, VIs, NDTIs, and LAI from observations (144 samples) were split into training and testing datasets, with 70% for training and 30% for testing. To validate the models' efficiency, a repeated resampling process of 10-fold cross-validation was used for training. Both performance and accuracy of each model were assessed, using the following metrics: R^2 and RMSE and can be expressed, accordingly:

$$R^2 = 1 - \frac{\sum_{i=1}^{n}(y_{obs}-y_{pred})^2}{\sum_{i=1}^{n}(y_{obs}-y)^2} \tag{9}$$

$$RMSE = \sqrt{\frac{1}{2}\sum_{i=1}^{n}(y_{obs} - y_{pred})^2} \tag{10}$$

where y_{obs} is the actual value, y_{pred} is the predicted value, and n is the number of observations. R^2 measures the proportion of the variance in LAI, as explained by the model. The values closer to 1 represent the better model fitting. RMSE offers an intuitive measure of error, in the same unit as LAI.

4. RESULTS AND DISCUSSION

During the four critical growth stages of rice (TL, PI, BT, and FW), LAI was observed. A general increase in the average LAI was seen. The development of the rice canopy was characterized by the minimum (Min), maximum (Max), mean, and standard deviation (SD) values, at each stage. The variability of rice's LAI is revealed due to agricultural inputs, such as nitrogen fertilization, rice varieties, and rice growth stages (**Fig. 1 and Table 1**). A description of LAI field observations is detailed in **Table 5**.

Table 5.

Statistical description of rice LAI observations, at different growth stages.

Rice growth stage	Sample	LAI field observation value			
		Minimum	Maximum	Mean	SD
TL	36	4.05	9.52	6.65	1.70
PI	36	4.28	12.23	7.03	1.21
BT	36	6.37	14.95	9.81	1.55
FW	36	7.01	17.92	11.01	2.66
FS	144	4.05	17.92	8.63	2.61

In **Table 5**, TL reveals an initial mean LAI of 6.65 (SD = 1.70), ranging from 4.05 to 9.52, indicating moderate leaf area expansion over a modest range. During PI, mean LAI increased to 7.03 (SD = 1.21), with a minimum of 4.28 and a maximum of 12.23. This outcome denotes a stable yet slightly more varied canopy structure, as rice matures. As for BT, LAI growth became more pronounced. The mean LAI reached 9.81 (SD = 1.55), with values ranging from 6.37 to 14.95, thereby suggesting the significance of canopy expansion at this stage. FW exhibited the highest mean LAI at 11.01 (SD = 2.66), with values spanning from 7.01 to 17.92. Hence, maximum canopy density and the most significant fluctuation, among the stages, are displayed. The higher SD in FW indicates enhanced structural diversity in the rice canopy, which can result from environmental or biological factors at advanced growth. The FS dataset, encompassing all growth stages, provided an aggregated view with a mean LAI of 8.63 (SD = 2.61), a minimum of 4.05, and a maximum of 17.92. This cumulative analysis revealed a clear upward trend in mean LAI values from TL to FW. As such, it can indicate progressive increase in leaf area, as rice develops. The FS dataset's broader range and higher SD displayed natural variability in LAI, across growth stages. Li et al. (2019) implies that the considerable variability in LAI, within and across different growth stages, is expected to encompass a broad range of possible methods, enabling it to evaluate the potential of UAV-based images in estimating rice LAI.

For broader applications, dataset size could pose limitations. Variability in physical conditions and agricultural practices across regions can influence model performance (Li et al., 2019; Wang et al., 2022). Additionally, large-scale implementation may introduce inconsistencies due to UAV flight parameters, sensor calibration, and atmospheric conditions, affecting spectral and textural indices (Zheng et al., 2020; Liu et al., 2023). It is crucial, therefore, to prioritize incorporating multi-location datasets, integrating satellite imagery for long-term monitoring, and applying transfer learning techniques to improve model adaptability (Shen et al., 2024; Chan et al., 2022). Such advancements will strengthen the reliability of UAV-based LAI estimation across diverse agricultural settings.

In regions with high variability in soil reflectivity, such as after irrigation or rainfall, soil background removal becomes even more critical. Soil reflectance changes due to moisture content or soil type can affect indices' calculations, leading to discrepancies in LAI estimation (Almeida-Ñauñay et al., 2023; Liu et al., 2023). Using the RGBVI thresholds for soil removal minimizes these confounding factors, resulting in more reliable growth metrics (Gitelson et al., 2002; Wang et al., 2022). RGBVI can help ML models to be more efficient when dealing with LAI and predictions. When computing the spectral index, this experiment minimized interference of the soil background.

4.1. Univariate ML modeling for LAI

The non-linear ML predictors (RFR, GBR, and XGBR) are associated with single CIs, VIs, and NDTIs, thereby demonstrating rice LAI, at each growing stage. To validate the performance of the models, both R^2 and RMSE were estimated and then incorporated. Of all the evaluation metrics, XGBR demonstrated superior performance. Consequently, only the results derived from XGBR are presented. In **Fig. 4**, the predictive capability of ML models, for each of the CIs and VIs evaluated, using 10-fold cross-validation, is illustrated.

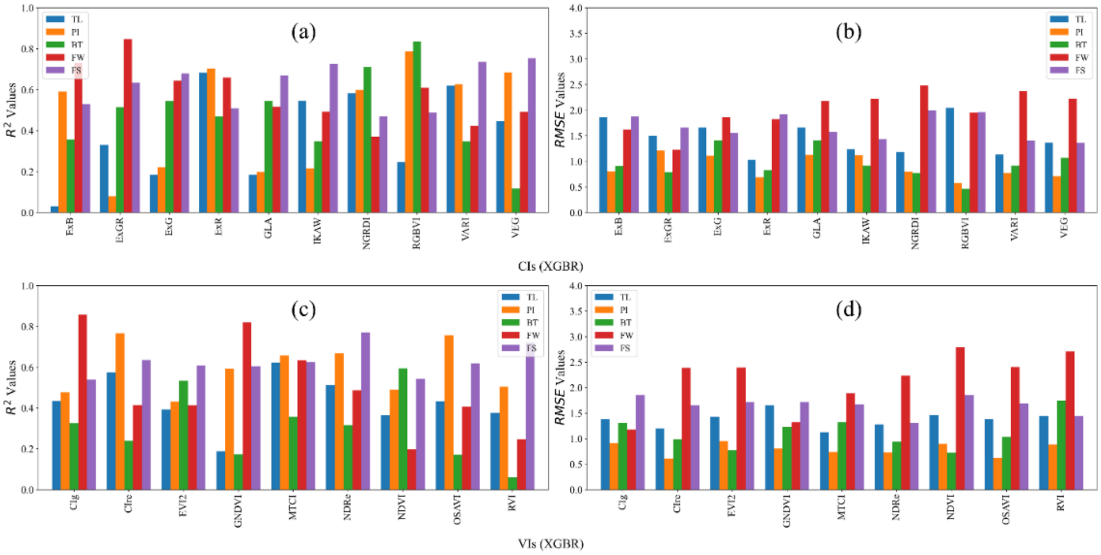

Fig. 4. The 10-fold cross-validated R^2 and RMSE of the CIs and VIs-based XGBR model exhibit the highest performance among its univariate models at each growth stage.

In **Fig. 4**, CI-based and VI-based XGBR predictive performance is presented. In the case of CIs, RGBVI is seen to demonstrate a strong relationship with LAI at each specific growth stage. Notably, it exhibits a robust correlation with LAI during BT, attaining 0.84 R^2 and 0.64 RMSE (**Fig. 4a and b**). ExGR also exhibits the highest R^2 value during FW. Nevertheless, its high RMSE suggests considerable variability in predictions. This discrepancy may arise from several factors e.g. light intensity and angle, soil reflectance, and structural variations of rice canopies (Wang et al., 2011; Gong et al., 2021; Sun et al., 2024). These factors contribute to the reduced effectiveness of CIs in reflecting LAI, during FW.

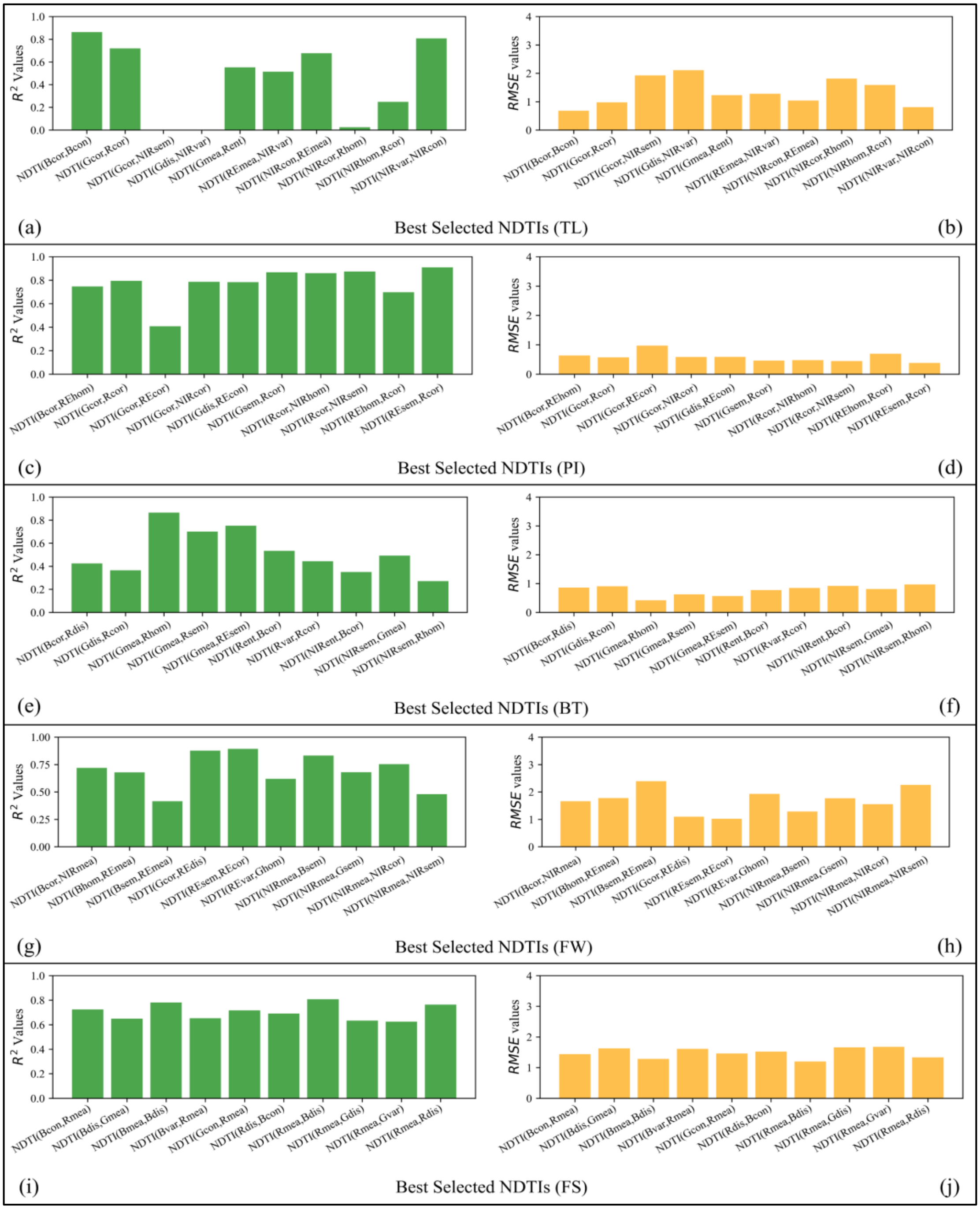

Fig. 5. Cross-validated R2 and RMSE of NDTI-based XGBR models for rice LAI estimation at (a – b) TL, (c – d) PI, (e - f) BT, (g – h) FW, and (i – j) FS, respectively.

The VIs-based model also reveals varying predictive performance across indices and growth stages (**Fig. 4c and d**). Three indices: CIg, GNDVI, and CIre indicate high R^2 values, though their RMSE values display differences in predictive accuracy. During FW, CIg reports the highest R^2 of 0.86, which signals a robust overall relationship with LAI. GNDVI also reports a high R^2 in the identical FW as CIg, attaining 0.82. CIg and GNDVI also report relatively high RMSEs of 1.18 and

1.33, respectively, which indicates considerable variability in prediction performance. Due to the heterogeneity of the canopy structure and related factors during FW, inconsistencies may occur (Prabhakar et al., 2024). During PI, however, CIre reveals a slightly lower R^2 of 0.77, and a significantly lower RMSE of 0.61. Considering both R^2 and RMSE, CIg demonstrates more consistent and accurate predictions. CIg is robust in capturing LAI variability during PI when the rice canopy is more uniform (Du et al., 2024).

According to CIs and VIs, our experiment found that VIs demonstrated the highest performance in reflecting LAI during BT. This accomplishment is attributed to the high chlorophyll content in rice leaves at this stage, which boosts the ability of VIs to reflect LAI due to increased efficiency in visible light absorption. Besides, this stage coincides with the peak growth of the flag leaf, resulting in a dense and uniform rice canopy, allowing VIs to reflect LAI with maximum accuracy (Zheng et al., 2020; Gong et al., 2021). In contrast, when comparing VIs' performance during FW, their effectiveness in reflecting LAI declines. This reduction is referred to as a decrease in chlorophyll content due to leaf senescence and changes in the structure of rice panicles, which tend to decline during this stage. These structural changes lead to significant fluctuations in NIR reflectance (Gong et al., 2021). For example, during FW, indices such as CIg and CNDVI exhibit high R^2 values, but their RMSE values are notably higher.

Integrating two distinct textures for constructing NDTI underscores a viable approach for predicting LAI. In this experiment, each of the five spectral bands is associated with extracting eight GLCM textures. At each growing stage, there are 1,460 NDTIs. Thus, the best ten high-predictive performance NDTIs were selected and reported. In **Fig. 5**, five distinct sets of evaluation metrics are presented. However, in TL, the predictive model's performance is diminished (**Fig. 5a and b**). On the other hand, PI is seen to demonstrate the most significant predictive outcomes. Notably, NDTI(REsem, Rcor) achieved 0.91 R^2 and recorded the lowest RMSE of 0.38 (**Fig. 5c and d**). During BT, NDTI(Gmea, Rhom) recorded 0.87 R^2 and RMSE of 0.42 (**Fig. 5e and f**). Results show that the NDTI-based XGBR model delivered better results during PI, demonstrating a strong correlation between R^2 and RMSE and expressing consistent performance, concerning the chosen NDTIs. In contrast, BT presents a denser and more complex canopy structure due to the development of rice panicles and a reduction in chlorophyll content at canopy level (Zheng et al., 2020). During BT, these factors may disrupt canopy uniformity and reduce the accuracy and consistency of NDTIs in reflecting LAI. FW (**Fig. 5g and h**) and FS (**Fig. 5i and j**) exhibit considerable consistency in both R^2 and RMSE values. It is significant that FS addresses the high consistency of predictive capability. During FS, the R^2 values of the selected NDTIs were found to be consistently above 0.62. The corresponding RMSE values were also higher than in PI. Consequently, the R^2 values demonstrated huge variability across the four growth stages. It is noted that most single variables delivered poor evaluations, reflecting stage-specific differences in model performance. However, the results of the univariate model across the growth stages revealed the most consistency. In **Table 6**, the top three best performances of the CI-based, VI-based, and NDTI-based XGBR models are reported. Therefore, nine XGBR models were selected as representatives of the univariate index-based models.

In **Table 6**, the top three results of the index-based XGBR models are shown. This combination, evaluated by the cross-validated R^2 and RMSE, reveals the highest predictive performance against all other ML counterparts for every univariate index. CI-based LAI estimation also achieved the best performance when associated with VEG. This combination resulted in 0.75 R^2 and RMSE of 1.36. As for VI, the top performance was observed with XGBR and NDRe variables, reaching 0.77 R^2 and RMSE of 1.28, indicating the most effective choice for the VI-based category. VIs are seen to derive their values from multispectral sensors, incorporating NIR, RE, and RGB bands. This broader spectral range offers VIs deeper insights into vegetation physiology and biochemical properties than CIs (Lu et al., 2022; Yu et al., 2023).

XGBR combined with NDTI(Rmea, Bdis) attained the highest performance among other univariate NDTI variables, recording 0.81 R^2 and RMSE of 1.20, revealing optimal predictive accuracy. During the FS stage, the superiority of indices-based XGBR is revealed, when associated with a single variable. In addition to the varying ability of different indices that reflect LAI across growth stages, it is evident that high R^2 values are observed alongside high RMSE values, in some cases. This phenomenon is frequently seen in several instances across all three indices. Therefore, R^2 alone may not fully capture the accuracy or reliability of the estimation (Wang et al., 2019a). It is, therefore, vital to consider both R^2 and RMSE together when evaluating the performance of a model.

Table 6.
The top three best performances of CIs, VIs, and NDTIs univariate XGBR models, across all growth stages based on training datasets with 10-fold cross-validation.

Index	Rational variable	R^2	RMSE
CIs	VEG	**0.75**	**1.36**
	VARI	0.74	1.41
	IKAW	0.73	1.43
VIs	NDRe	**0.77**	**1.28**
	RVI	0.72	1.45
	CIRe	0.64	1.65
NDTIs	NDTI(Rmea, Bdis)	**0.81**	**1.20**
	NDTI(Bmea, Bdis)	0.78	1.28
	NDTI(Rmea, Rdis)	0.76	1.33

4.2 Multivariate ML modeling for LAI

In this section, all model inputs are divided into CIs, VIs, NDTIs, CIs + VIs, CIs + NDTIs, VIs + NDTIs, and CIs + VIs + NDTIs. Employing all available features in predictive modeling can lead to excessive inter-correlation among them. This redundancy can diminish the reliability of the models and increase the risk of overfitting. Moreover, the model may only capture specific data patterns, which can reduce its performance when making predictions on testing data (Chan et al., 2022). Such repetition may elevate standard errors and increase the variance of coefficients. As a result, the model's accuracy can be decreased, affecting overall predictive performance (Shrestha, 2020).

To increase the predictive performance of estimating LAI, feature selection and dimensional reduction approaches were employed by selecting the most informative features. In our experiment, RFE was applied along with RFR, GBR, and XGBR to determine the most pertinent indices that provide the highest predictive performance (Darst et al., 2018). In **Table 7**, a comparison of multivariate models' performance is outlined, and measured by cross-validated metrics (R^2 and RMSE). Concurrently, dimensional reduction techniques (PCR and PLSR) were employed to tackle the challenges associated with multicollinearity and high-dimensional datasets. These techniques converted the original variables into fewer components, preserving the most substantial variance or covariance with LAI. In **Fig. 6**, results of multivariate models, including RFR (blue-dashed line), GBR (orange-dashed line), XGBR (green-dashed line), PCR (red-dashed line), and (purple-dashed line), which sample different feature numbers to estimate LAI, are stated. To measure performance, evaluation utilizes statistical metrics (R^2 and RMSE).

In **Table 7**, the predictive performances of total and selected features, using RFE, are depicted. CIs reveal the highest predictive performance for total feature (10 features) predictions, attaining 0.85 R^2 and 1.06 RMSE, respectively. It is also noted that XGBR and GBR can deliver better accuracy than RF when associated with single and combined indices, in the acceptable range for all models. After applying the feature selection, predictive results improve significantly. Both CIs and CIs + VIs demonstrate the highest predictive performance, achieving 0.88 R^2 equally. For RMSE, CIs attained 0.94 RMSE, compared to CIs + VIs, which exhibited 0.96 RMSE: a slight difference. However, the number of features indicated that only 5 selected features out of 10 could deliver the highest accuracy for CIs. In comparison, CIs + VIs need 12 features out of 19 to increase the performance of the model's prediction. These results signify that applying RFE can enhance the predictive performance of the models by improving R^2 and RMSE. Reducing the number of the model's inputs also benefits the computational complexity.

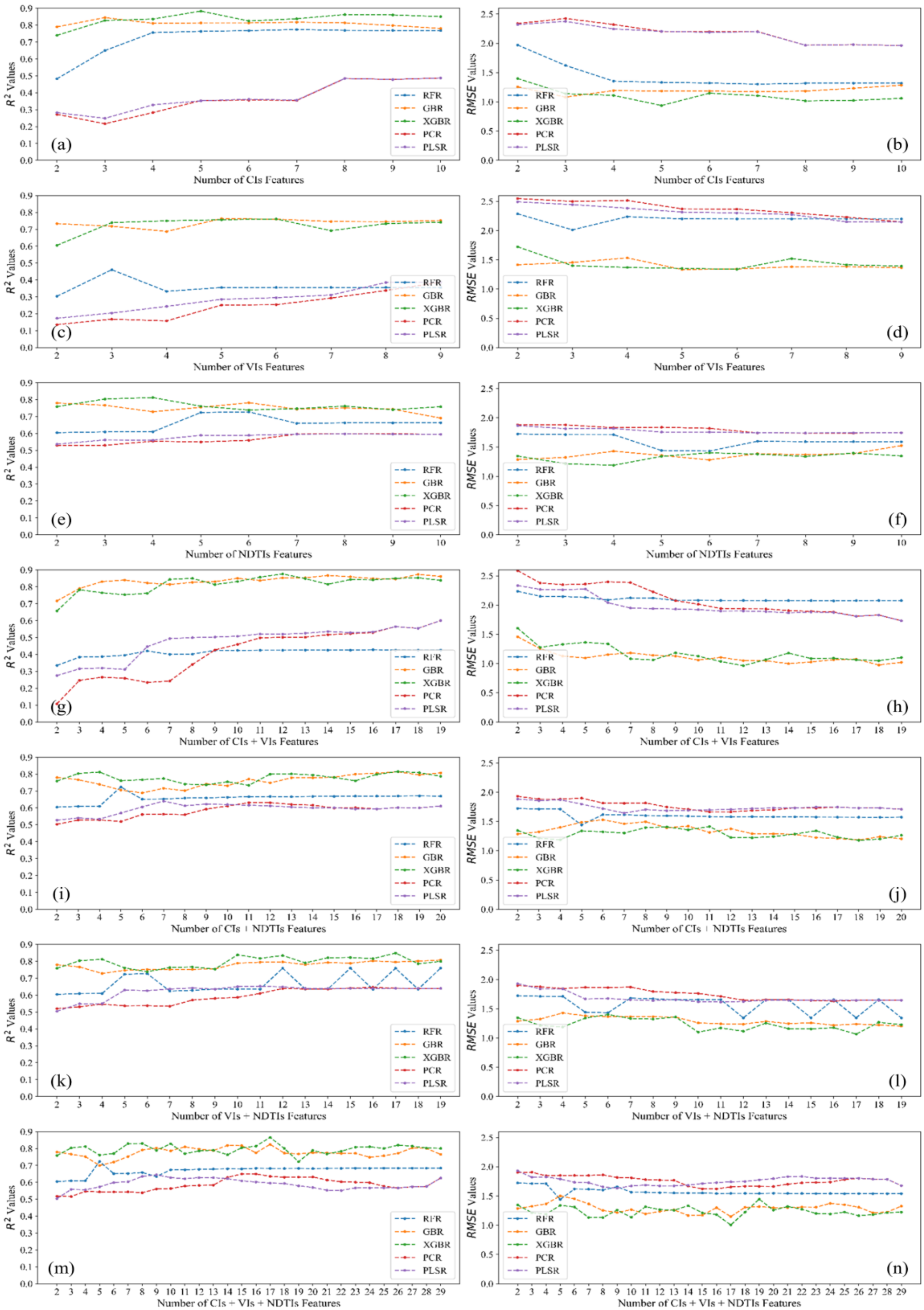

Fig. 6. Performance comparison of univariate and multivariate models for LAI estimation, using RFE and dimensional reduction.

Table 7.

Comparison of multivariate models' performance utilizing RFE to ML models.

Index	Model	Total features	R^2	RMSE	Model	Selected features	R^2	RMSE
CIs	XGBR	10	0.85	1.06	XGBR	5	0.88	0.94
VIs	GBR	9	0.75	1.37	XGBR	6	0.76	1.34
NDTIs	XGBR	10	0.76	1.35	XGBR	4	0.81	1.19
CIs + VIs	XGBR	19	0.84	1.10	XGBR	12	0.88	0.96
CIs + NDTIs	GBR	20	0.80	1.57	XGBR	18	0.81	1.18
Vis + NDTIs	GBR	19	0.81	1.23	XGBR	17	0.85	1.07
CIs + VIs + NDTIs	XGBR	29	0.80	1.22	XGBR	17	0.87	1.00

According to **Fig. 6**, RFR, GBR, and XGBR exhibit superior performance compared to PCR and PLSR. Dimensional reduction models yield lower R^2 and exhibit higher RMSE in every quantity of feature input. XGBR demonstrated the most favorable performance along with CIs among its counterparts, attaining five features to achieve 0.88 R^2 and 0.94 RMSE (**Fig. 6a and b**). In contrast, for VIs, RFR's performance diminished similarly to that of PCR and PLSR, resulting in lower R^2 and increased RMSE. XGBR, however, performed the best with VIs, employing six features, resulting in 0.76 R^2 and RMSE of 1.34 (**Fig. 6c and d**). When assessing NDTIs, both PCR and PLSR significantly amplified predictive performance. Nonetheless, XGBR secured the best results for NDTIs, as presented in **Fig. 6e and f**. Utilizing four features yielded 0.81 R^2 and RMSE of 1.19.

In **Fig. 6g and h**, the combination of CIs and VIs is explored. Such a combination points to a detrimental effect of VIs on the performance of RFR while failing to improve the performance of PCR and PLSR. In this scenario, XGBR achieved optimal results. Twelve features were utilized, reaching 0.88 R^2 and RMSE of 0.96. Similar enhancements in PCR and PLSR predictive performance are observed for CIs + NDTIs (**Fig. 6i and j**) and VIs + NDTIs (**Fig. 6k and l**). When CIs + NDTIs are merged, XGBR achieved the best outcomes, employing eighteen features, realizing 0.81 R^2 and RMSE of 1.18. Similarly, when VIs + NDTIs are merged, XGBR demonstrated superior performance, using seventeen features, achieving 0.85 R^2 and RMSE of 1.07.

In **Fig. 6m and n**, the combination of all three feature groups (CIs + VIs + NDTIs) are assessed. In this evaluation, XGBR retained the highest performance (0.87 R^2 and 1.00 RMSE) employing seventeen features. Overall, XGBR consistently demonstrated the best predictive performance compared to other models. The features' number and combination of indices much influenced each model's ability to estimate LAI.

The performance of LAI estimation, among the models RFR, GBR, XGBR, PCR, and PLSR, was compared. Using all available features, both GBR and XGBR models outperformed the others. However, when RFE was applied to select only the most important features for model learning, the XGBR model surpassed all other models' performance. This improvement was demonstrated by an increase in R^2, a decrease in RMSE, and a reduction in the number of features used. Both single and combined index scenarios showed that RFE enhanced the effectiveness of XGBR. As shown in **Table 7**, in the case of CIs + VIs + NDTIs, R^2 increased from 0.80 to 0.87, RMSE decreased from 1.22 to 1.00, and the number of features reduced from 29 to only 17.

Shen et al. (2024) states that using all features in a model does not necessarily yield better performance and may result in suboptimal statistical metrics. This phenomenon is likely due to the inclusion of irrelevant or redundant features in the model's learning process, which RFE effectively mitigates (Shrestha, 2020; Chan et al., 2022). In estimating LAI, RFE is seen to improve the efficiency of XGBR. According to **Table 7**, after using RFE to select only essential features, the estimation of LAI, using only 5 CIs features, provided superior statistical performance compared to other indices (Darst et al., 2018). While R^2 values for CIs and CIs + VIs (12 features) are comparable, when considering RMSE, CIs performed slightly better, with RMSE of 0.94, compared to 0.96 for CIs + VIs. This outcome demonstrates that feature selection with RFE can augment model performance by reducing redundancy and focusing on the most critical variables, particularly for the XGBR model.

In **Fig. 6**, PLSR and PCR perform statistically worse on VIs and CIs than other models. These models cannot adequately capture the variability inherent in these indices. The primary reason is that the relationship between LAIs and VIs is not always linear. Specifically, VIs are influenced by various factors, such as temperature, soil moisture, and the vegetation phenological stage, all of which impact the characteristics of the vegetation canopy. These factors alter the absorption and scattering of light depending on the direction and density of the canopy (Qiao et al., 2019). Besides, the chlorophyll content of plants, which varies with phenological stages, affects the sensitivity of red-edge spectral reflectance (Xie et al., 2018).

Similarly, CIs are influenced by external factors, resulting in variability that affects LAI estimation. By design, PCR tends to remove low-variance variables from the dataset. While this helps mitigate overfitting, PCR does not consider whether the removed variables are essential to the predicted dependent variable. As a result, PCR struggles to handle non-linear data. In contrast, PLSR reduces the weight of less important features rather than removing them entirely. Yet, these low-importance features can still introduce noise, adversely affecting the model's predictive ability, thus reducing accuracy (Hastie et al., 2009). On the other hand, ensemble tree models are inherently better suited to capturing non-linear relationships.

Incorporating texture features with spectral indices can expedite the performance of PCR and PLSR in LAI estimation. As shown in **Fig. 6k**, when using VIs + NDTIs, the R^2 values for these models improve. Such higher values arise because VIs often exhibit increased variability due to changes in canopy characteristics such as density, especially from BT to FW. Texture features mitigate the saturation effect in VIs caused by reflectance variability and help distinguish the complex structures of the canopy (Zhou et al., 2022). In the case of CIs, which are often affected by illumination differences, texture features reduce noise by analyzing pixel intensity differences. This ability helps minimize the noise caused by varying reflectance within the canopy (Zheng et al., 2020; Zou et al., 2024), thereby fine-tuning the overall performance of the models.

Although CIs may be sensitive to various factors, their integration with ML techniques boosts both accuracy and efficiency of LAI estimation, mainly when researchers apply ensemble models like XGBR (Ilniyaz et al., 2022). It is noted that multispectral UAV sensors cost significantly more than those using RGB bands (Yamaguchi et al., 2020). Consequently, researchers can use RGB bands as a cost-effective yet accurate alternative for LAI estimation, providing an efficient solution for precision agriculture while reducing operational costs. UAV's implementation in resource-constrained agricultural settings presents several challenges. The high cost of multispectral UAV sensors and data processing infrastructure can limit accessibility for smallholder farmers (Wang et al., 2022). Factors, such as limited technical expertise, regulatory restrictions on UAV operations, and the need for frequent sensor calibration can also hinder large-scale deployment (Liu et al., 2023). In areas with inconsistent internet connectivity, real-time data processing and cloud-based storage may not be feasible, necessitating the development of offline, user-friendly analytical tools (Shen et al., 2024).

In this work, one primary limitation is the dataset size, as previously discussed, which is restricted to a specific region and environmental conditions. These issues can be regarded as potential sources of error (Wang et al., 2022). Expanding the dataset to include multiple regions with diverse agricultural conditions would improve model robustness and scalability. Sensor limitations and UAV flight conditions, however, may introduce sources of error. Variations in illumination, atmospheric conditions, and sensor calibration can greatly affect model accuracy (Liu et al., 2023). While preprocessing techniques can be applied to correct these effects, residual errors may persist. Moreover, ML model performance can vary based on the selected indices and feature selection process. Although RFE is seen to promote model efficiency, specific relevant indices might have been excluded, potentially influencing predictive accuracy (Zhang et al., 2020).

The findings of this study have significant implications for precision agriculture, particularly in optimizing resource allocation, improving crop monitoring, and facilitating decision-making frameworks. The integration of UAV-derived spectral and texture indices with ML models enables high-resolution, stage-specific LAI estimation, thus supporting more efficient irrigation scheduling, nutrient management, and early stress detection in rice cultivation (Wang et al., 2022). The demonstrated cost-effectiveness of UAV-based RGB-derived indices offers a viable alternative for smallholder farmers. Such a strategy can potentially reduce barriers to adopting precision agriculture technologies. Scaling these approaches through government-led digital agriculture initiatives could accelerate real-time crop monitoring, promoting data-driven policies that enhance food security and climate resilience (Shen et al., 2024).

To evaluate its transferability and robustness under varying conditions, future efforts should apply this methodology across a broader range of experiments, such as species diversity and differences in image resolution. Expanding its applicability to diverse agricultural contexts will ensure the adaptability and reliability of the proposed models. Ultimately, the focus should be on incorporating larger datasets and exploring advanced modeling techniques to refine these methodologies, improving both their accuracy and scalability in real-world applications.

5. CONCLUSION

In this paper, results demonstrate the effectiveness of UAV-based remote sensing data for accurately estimating LAI across multiple growth stages of rice. Critical insights into the performance of various indices and ML models were identified through a comprehensive evaluation of univariate and multivariate modeling approaches. Univariate analysis revealed that VIs and NDTIs exhibit strong correlations with LAI during specific growth stages. For instance, indices such as CIg and ExGR demonstrated high R^2 values during FW. At the same time, NDTIs, including NDTI(REsem, Rcor) and NDTI(Gmea, Rhom), achieved exceptional performance during PI and BT, respectively. In some instances, elevated RMSE values highlighted the limitations of single-variable models in capturing stage-specific variability. In contrast, multivariate models incorporating RFE and dimensional reduction techniques, such as PCR and PLSR, exhibited superior predictive performance. Among these, XGBR emerged as the most reliable model, consistently delivering high R^2 values and low RMSE, across various index combinations. The integration of CIs, VIs, and NDTIs within multivariate frameworks enhanced the accuracy of predictions, particularly in stage-specific contexts where canopy complexity presented additional challenges. These findings emphasize the importance of combining spectral and texture indices with advanced ML models for precise LAI estimation. Furthermore, this study provides a robust methodological framework for integrating UAV-based data into precision agriculture practices, facilitating stage-specific monitoring and informed decision-making.

ACKNOWLEDGEMENTS

This research was funded by the Faculty of Liberal Arts' Research Fund, Thammasat University, Fiscal year 2566, Contract No. 1/2566. It is also supported by the Faculty of Liberal Arts, Thammasat University, Research Unit in Geospatial Applications (Capybara Geo Lab).

REFERENCES

Abdullah, A.N.H., Muharam, F.M., Zulkafli, Z.D., Nurulhuda, K., Hashim, M.F.C., Zad, S.N.M., & Ismail, M.R., (2019) Estimation of leaf area index from UAV multispectral indices and machine learning models. *Proceedings of the 40th Asian Conference on Remote Sensing (ACRS 2019).* pp. MoA1-2. ACRS.

Almeida-Ñauñay, A.F., Tarquis, A.M., López-Herrera, J., Pérez-Martín, E., Pancorbo, J.L., Raya-Sereno, M.D. & Quemada, M. (2023) Optimization of soil background removal to improve the prediction of wheat traits with UAV imagery. *Computers and Electronics in Agriculture*, *205*, p.107559. https://doi.org/10.1016/j.compag.2022.107559

Afrasiabian, Y., Mokhtari, A., & Yu, K. (2022) Machine Learning on the estimation of Leaf Area Index. 42. GIL-Jahrestagung, Künstliche Intelligenz in der Agrar-und Ernährungswirtschaft. https://dl.gi.de/items/e390ee01-6e52-46a0-b4a6-753202fc8a14

Bréda, N.J. (2003) Ground-based measurements of leaf area index: a review of methods, instruments and current controversies. *Journal of experimental botany*, *54*(392), pp.2403-2417. https://doi.org/10.1093/jxb/erg263

Brieman, L. (2001) Random forests. *Machine learning*, *45*, pp.5-32.

Cao, Y., Li, G.L., Luo, Y.K., Pan, Q. & Zhang, S.Y. (2020) Monitoring of sugar beet growth indicators using wide-dynamic-range vegetation index (WDRVI) derived from UAV multispectral images. *Computers and Electronics in Agriculture*, *171*, p.105331. https://doi.org/10.1016/j.compag.2020.105331

Chan, J.Y.L., Leow, S.M.H., Bea, K.T., Cheng, W.K., Phoong, S.W., Hong, Z.W. & Chen, Y.L. (2022) Mitigating the multicollinearity problem and its machine learning approach: a review. *Mathematics*, *10*(8), p.1283. https://doi.org/10.3390/math10081283

Chen, T., & Guestrin, C. (2016) Xgboost: A scalable tree boosting system. *Proceedings of the 22nd acm sigkdd international conference on knowledge discovery and data mining*. pp. 785-794.

Darst, B.F., Malecki, K.C. & Engelman, C.D. (2018) Using recursive feature elimination in random forest to account for correlated variables in high dimensional data. *BMC genetics*, *19*, pp.1-6. https://doi.org/10.1186/s12863-018-0633-8

Du, X., Zheng, L., Zhu, J. & He, Y., (2024) Enhanced Leaf Area Index Estimation in Rice by Integrating UAV-Based Multi-Source Data. *Remote Sensing*, *16*(7), p.1138. https://doi.org/10.3390/rs16071138

Fabian, P. (2011) Scikit-learn: Machine learning in Python. *Journal of machine learning research 12*, p.2825.

Fukuda, S., Koba, K., Okamura, M., Watanabe, Y., Hosoi, J., Nakagomi, K., Maeda, H., Kondo, M. & Sugiura, D. (2021) Novel technique for non-destructive LAI estimation by continuous measurement of NIR and PAR in rice canopy. *Field Crops Research*, *263*, p.108070. https://doi.org/10.1016/j.fcr.2021.108070

Gitelson, A.A., Kaufman, Y.J., Stark, R. & Rundquist, D. (2002) Novel algorithms for remote estimation of vegetation fraction. *Remote sensing of Environment, 80*(1), pp.76-87. https://doi.org/10.1016/S0034-4257(01)00289-9

Gong, Y., Yang, K., Lin, Z., Fang, S., Wu, X., Zhu, R., & Peng, Y. (2021) Remote estimation of leaf area index (LAI) with unmanned aerial vehicle (UAV) imaging for different rice cultivars throughout the entire growing season. *Plant Methods, 17*(1), p.88. https://doi.org/10.1186/s13007-021-00789-4

Hastie, T., Tibshirani, R., Friedman, J. & Franklin, J. (2009) The elements of statistical learning: data mining, inference and prediction. 2nd edn. New York: Springer.

Hikosaka, K. (2005). Leaf canopy as a dynamic system: Ecophysiology and optimality in leaf turnover. *Annals of botany*, *95*(3), pp.521-533. https://doi.org/10.1093/aob/mci050

Ilniyaz, O., Kurban, A. & Du, Q. (2022) Leaf area index estimation of pergola-trained vineyards in arid regions based on UAV RGB and multispectral data using machine learning methods. *Remote Sensing, 14*(2), p.415. https://doi.org/10.3390/rs14020415

Kamthonkiat, D., Honda, K., Turral, H., Tripathi, N., & Wuwongse, V. (2005) Discrimination of irrigated and rainfed rice in a tropical agricultural system using SPOT VEGETATION NDVI and rainfall data. *International Journal of Remote Sensing*, *26*(12), pp.2527-2547. https://doi.org/10.1080/01431160500104335

Kappas, M. W., & Propastin, P. A. (2012) Review of available products of leaf area index and their suitability over the formerly soviet central Asia. *Journal of Sensors*, *2012*(1), p.582159. https://doi.org/10.1155/2012/582159

Li, S., Yuan, F., Ata-UI-Karim, S. T., Zheng, H., Cheng, T., Liu, X., Tian, Y., Zhu, Y., Cao, W. & Cao, Q. (2019) Combining color indices and textures of UAV-based digital imagery for rice LAI estimation. *Remote Sensing, 11*(15), p.1763. https://doi.org/10.3390/rs11151763

Liu, S., Jin, X., Nie, C., Wang, S., Yu, X., Cheng, M., Shao, M., Wang, Z., Tuohuti, N., Bai, Y. & Liu, Y. (2021) Estimating leaf area index using unmanned aerial vehicle data: shallow vs. deep machine learning algorithms. *Plant Physiology, 187*(3), pp.1551-1576. https://doi.org/10.1093/plphys/kiab322

Liu, S., Jin, X., Bai, Y., Wu, W., Cui, N., Cheng, M., Liu, Y., Meng, L., Jia, X., Nie, C. & Yin, D. (2023) UAV multispectral images for accurate estimation of the maize LAI considering the effect of soil background. *International Journal of Applied Earth Observation and Geoinformation, 121*, p.103383. https://doi.org/10.1016/j.jag.2023.103383

Lu, Z., Deng, L. & Lu, H. (2022) An improved LAI estimation method incorporating with growth characteristics of field-grown wheat. *Remote Sensing, 14*(16), p.4013. https://doi.org/10.3390/rs14164013

Prabhakar, M., Gopinath, K. A., Ravi Kumar, N., Thirupathi, M., Sai Sravan, U., Srasvan Kumar, G., Samba Siva, G., Chandana, P. & Singh, V. K. (2024) Mapping Leaf Area Index at Various Rice Growth Stages in Southern India Using Airborne Hyperspectral Remote Sensing. *Remote Sensing, 16*(6), p.954. https://doi.org/10.3390/rs16060954

Qiao, K., Zhu, W., Xie, Z., & Li, P. (2019) Estimating the seasonal dynamics of the leaf area index using piecewise LAI-VI relationships based on phenophases. *Remote Sensing, 11*(6), p.689. https://doi.org/10.3390/rs11060689

Sanches, G. M., Duft, D. G., Kölln, O. T., Luciano, A. C. D. S., De Castro, S. G. Q., Okuno, F. M., & Franco, H. C. J. (2018) The potential for RGB images obtained using unmanned aerial vehicle to assess and predict yield in sugarcane fields. *International journal of remote sensing, 39*(15-16), pp.5402-5414. https://doi.org/10.1080/01431161.2018.1448484

Shen, Y., Yan, Z., Yang, Y., Tang, W., Sun, J., & Zhang, Y. (2024) Application of UAV-Borne Visible-Infared Pushbroom Imaging Hyperspectral for Rice Yield Estimation Using Feature Selection Regression Methods. *Sustainability, 16*(2), p.632. https://doi.org/10.3390/su16020632

Shrestha, N. (2020) Detecting multicollinearity in regression analysis. *American Journal of Applied Mathematics and Statistics, 8*(2), pp.39-42. https://doi.org/10.12691/ajams-8-2-1

Singkawat, C., & Intarat, K. (2024) Rice Cropping Systems Classification using Time-Series Landsat Images and Phenology-Based Algorithms in Suphan Buri, Thailand. *Asia-Pacific Journal of Science and Technology, 29*(1), p.10. https://doi.org/10.14456/apst.2024.10

Sun, B., Li, Y., Huang, J., Cao, Z., & Peng, X. (2024) Impacts of Variable Illumination and Image Background on Rice LAI Estimation Based on UAV RGB-Derived Color Indices. *Applied Sciences*, *14*(8), p.3214. https://doi.org/10.3390/app14083214

Wang, F. M., Huang, J. F., & Lou, Z. H. (2011) A comparison of three methods for estimating leaf area index of paddy rice from optimal hyperspectral bands. *Precision Agriculture, 12*, pp.439-447. https://doi.org/10.1007/s11119-010-9185-2

Wang, L., Chang, Q., Li, F., Yan, L., Huang, Y., Wang, Q., & Luo, L. (2019a) Effects of growth stage development on paddy rice leaf area index prediction models. *Remote Sensing, 11*(3), p.361. https://doi.org/10.3390/rs11030361

Wang, Y., Zhang, K., Tang, C., Cao, Q., Tian, Y., Zhu, Y., ... & Liu, X. (2019b) Estimation of rice growth parameters based on linear mixed-effect model using multispectral images from fixed-wing unmanned aerial vehicles. *Remote sensing, 11*(11), p.1371. https://doi.org/10.3390/rs11111371

Wang, W., Zheng, H., Wu, Y., Yao, X., Zhu, Y., Cao, W., & Cheng, T. (2022) An assessment of background removal approaches for improved estimation of rice leaf nitrogen concentration with unmanned aerial vehicle multispectral imagery at various observation times. *Field Crops Research, 283*, p.108543. https://doi.org/10.1016/j.fcr.2022.108543

Watson, D. J. (1947) Comparative physiological studies on the growth of field crops: I. Variation in net assimilation rate and leaf area between species and varieties, and within and between years. *Annals of Botany, 11*(1), pp.41-76. https://doi.org/10.1093/oxfordjournals.aob.a083148

Xie, Q., Dash, J., Huang, W., Peng, D., Qin, Q., Mortimer, H., Casa, R., Pignatti, S., Laneve, G., Pascucci, S. & Dong, Y. (2018) Vegetation indices combining the red and red-edge spectral information for leaf area index retrieval. *IEEE Journal of selected topics in applied earth observations and remote sensing, 11*(5), pp.1482-1493. https://doi.org/10.1109/JSTARS.2018.2813281

Xue, J., & Su, B. (2017) Significant remote sensing vegetation indices: A review of developments and applications. *Journal of sensors, 2017*(1), p.1353691. https://doi.org/10.1155/2017/1353691

Yamaguchi, T., Tanaka, Y., Imachi, Y., Yamashita, M., & Katsura, K. (2020) Feasibility of combining deep learning and RGB images obtained by unmanned aerial vehicle for leaf area index estimation in rice. *Remote Sensing, 13*(1), p.84. https://doi.org/10.3390/rs13010084

Yan, G., Hu, R., Luo, J., Weiss, M., Jiang, H., Mu, X., Xie, D. & Zhang, W. (2019) Review of indirect optical measurements of leaf area index: Recent advances, challenges, and perspectives. *Agricultural and Forest Meteorology, 265*, pp.390-411. https://doi.org/10.1016/j.agrformet.2018.11.033

Yang, K., Gong, Y., Fang, S., Duan, B., Yuan, N., Peng, Y., Wu, X. & Zhu, R. (2021) Combining spectral and texture features of UAV images for the remote estimation of rice LAI throughout the entire growing season. *Remote Sensing, 13*(15), p.3001. https://doi.org/10.3390/rs13153001

Yu, T., Zhou, J., Fan, J., Wang, Y. & Zhang, Z. (2023) Potato leaf area index estimation using multi-sensor unmanned aerial vehicle (uav) imagery and machine learning. *Remote Sensing, 15*(16), p.4108. https://doi.org/10.3390/rs15164108

Yuan, H., Yang, G., Li, C., Wang, Y., Liu, J., Yu, H., Feng, H., Xu, B., Zhao, X., & Yang, X. (2017) Retrieving soybean leaf area index from unmanned aerial vehicle narrowband multispectral remote sensing: Analysis of RF, ANN, and SVM regression models. *Remote Sensing, 9*(4), p.309. https://doi.org/10.3390/rs9040309

Zeng, X., Chen, Y. W., & Tao, C. (2009) Feature selection using recursive feature elimination for handwritten digit recognition. In *2009 Fifth International Conference on Intelligent Information Hiding and Multimedia Signal Processing*, September, pp. 1205-1208. IEEE.

Zhang, Y., Yang, Y., Zhang, Q., Duan, R., Liu, J., Qin, Y., & Wang, X. (2022a) Toward multi-stage phenotyping of soybean with multimodal UAV sensor data: a comparison of machine learning approaches for leaf area index estimation. *Remote Sensing, 15*(1), p.7. https://doi.org/10.3390/rs15010007

Zhang, F., Hassanzadeh, A., Kikkert, J., Pethybridge, S. J., & van Aardt, J. (2022b) Evaluation of Leaf Area Index (LAI) of Broadacre crops using UAS-Based LiDAR point clouds and multispectral imagery. *IEEE Journal of Selected Topics in Applied Earth Observations and Remote Sensing, 15*, pp.4027-4044. https://doi.org/10.1109/JSTARS.2022.3172491

Zheng, H., Cheng, T., Zhou, M., Li, D., Yao, X., Tian, Y., Cao, W. & Zhu, Y. (2019) Improved estimation of rice aboveground biomass combining textural and spectral analysis of UAV imagery. *Precision Agriculture, 20*, pp.611-629. https://doi.org/10.1007/s11119-018-9600-7

Zheng, H., Zhou, X., He, J., Yao, X., Cheng, T., Zhu, Y., Cao, W. & Tian, Y. (2020) Early season detection of rice plants using RGB, NIR-GB and multispectral images from unmanned aerial vehicle (UAV). *Computers and electronics in agriculture, 169*, p.105223. https://doi.org/10.1016/j.compag.2020.105223

Zhou, C., Gong, Y., Fang, S., Yang, K., Peng, Y., Wu, X., & Zhu, R. (2022) Combining spectral and wavelet texture features for unmanned aerial vehicles remote estimation of rice leaf area index. *Frontiers in Plant Science, 13*, p.957870. https://doi.org/10.3389/fpls.2022.957870

Zhu, W., Sun, Z., Huang, Y., Lai, J., Li, J., Zhang, J., Yang, B., Li, B., Li, S., Zhu, K., Li, Y. & Liao, X. (2019) Improving field-scale wheat LAI retrieval based on UAV remote-sensing observations and optimized VI-LUTs. *Remote Sensing, 11*(20), p.2456. https://doi.org/10.3390/rs11202456

Zou, M., Liu, Y., Fu, M., Li, C., Zhou, Z., Meng, H., Xing, E. & Ren, Y. (2024) Combining spectral and texture feature of UAV image with plant height to improve LAI estimation of winter wheat at jointing stage. *Frontiers in Plant Science*, *14*, p.1272049. https://doi.org/10.3389/fpls.2023.1272049